Journal of Power Sources 202 (2012) 253–261

Contents lists available at SciVerse ScienceDirect

Journal of Power Sources

journal homepage: www.elsevier.com/locate/jpowsour

Carbon coating to suppress the reduction decomposition of electrolyte on the $Li_4Ti_5O_{12}$ electrode

Yan-Bing He[a], Feng Ning[a,b], Baohua Li[a], Quan-Sheng Song[c], Wei Lv[c], Hongda Du[a], Dengyun Zhai[a,b], Fangyuan Su[c], Quan-Hong Yang[a,c,*], Feiyu Kang[a,b,*]

[a] Key Laboratory of Thermal Management Engineering and Materials, Graduate School at Shenzhen, Tsinghua University, Shenzhen 518055, China
[b] Laboratory of Advanced Materials, Department of Materials Science and Engineering, Tsinghua University, Beijing 100084, China
[c] Key Laboratory for Green Chemical Technology of Ministry of Education, School of Chemical Engineering and Technology, Tianjin University, Tianjin 300072, China

ARTICLE INFO

Article history:
Received 22 August 2011
Received in revised form
14 November 2011
Accepted 15 November 2011
Available online 9 December 2011

Keywords:
Lithium titanate
Carbon coating
Reduction decomposition
Electrolyte
Solid electrolyte interface film

ABSTRACT

The lithium ion batteries using $Li_4Ti_5O_{12}$ as the anode material are easily being inflated during charge and discharge, which, however, does not occur in the batteries using graphite as the anode material. The high reduction reactivity of electrolyte on the $Li_4Ti_5O_{12}$ material may be the main reason. In this work, the reduction reactivities of electrolyte on the uncoated and carbon-coated $Li_4Ti_5O_{12}$ electrodes are compared for the first time. The results show that the reduction decomposition of electrolyte does occur on the uncoated $Li_4Ti_5O_{12}$ electrode at around 0.7 V, while it only takes place at the first cycle on the carbon-coated $Li_4Ti_5O_{12}$ electrode. The carbon coating layers cover the catalytic active sites of $Li_4Ti_5O_{12}$ particles and separate the $Li_4Ti_5O_{12}$ particles from the electrolyte. A successive solid electrolyte interface (SEI) film is formed on the carbon layer during the formation process, which can prevent the further reduction decomposition of electrolyte at around 0.7 V. The impurity phases of rutile and anatase TiO_2 do not influence the reduction reactivity of electrolyte. This work is not only important to understand the reduction decomposition mechanism of electrolyte on the $Li_4Ti_5O_{12}$ electrode, but also provides an effective solution to suppress the reduction decomposition of electrolyte in the batteries.

1. Introduction

The spinel $Li_4Ti_5O_{12}$ material with a theoretical capacity of 175 mAh g^{-1} has excellent Li-ion intercalation/deintercalation reversibility within the voltage range of 2.5–1.0 V. $Li_4Ti_5O_{12}$ exhibits zero strain or volume change during charge and discharge cycles and excellent safety performance [1–3]. $Li_4Ti_5O_{12}$ also has a very flat voltage plateau at around 1.55 V (vs. Li/Li^+), which is higher than the reduction potential of most organic electrolytes [4–6]. $Li_4Ti_5O_{12}$ is therefore much safer and more stable than carbon-based materials. $Li_4Ti_5O_{12}$ has demonstrated the potential as a good candidate material for negative electrodes used in long life type lithium-ion power batteries.

However, it is found by battery manufacturers that the lithium ion batteries using $Li_4Ti_5O_{12}$ as anode material are easily being inflated during charge/discharge, especially at high-temperature condition, where the reduction gases such as hydrocarbon gases and CO are generated in the batteries. The same phenomenon hardly takes place in the batteries using graphite as the anode material. This has become a main obstacle for the use of $Li_4Ti_5O_{12}$ as anode material for the lithium ion power batteries. The inflation-based expansion of batteries leads to bad contact of positive and negative electrodes, which results in a significant increase of battery resistance. Hence, the battery performance will soon collapse. So far, extensive work has been done to improve the electrochemical performance of $Li_4Ti_5O_{12}$ material by preparing nanoparticles [7–10], doping [11–16] and forming composites with carbon and metal powder [14,17–22], whereas the gas generation of $Li_4Ti_5O_{12}$ anode batteries has not been paid enough attentions by researchers. The reason is that the researchers mainly use the $Li_4Ti_5O_{12}$/Li coin cells to characterize the performance of $Li_4Ti_5O_{12}$ materials within the voltage range of 2.5–1.0 V, which do not show the inflation behavior. However, for the commercial $Li_4Ti_5O_{12}$ anode batteries, especially the liquid state soft pack batteries, they are easily being inflated during cycling due to the gas generation in the batteries. The high reduction reactivity of electrolyte on the $Li_4Ti_5O_{12}$ electrode may be the main reason. However, there are no reports about the studies on the reduction reactivity of electrolyte on the $Li_4Ti_5O_{12}$ electrode to understand and prevent the gas generation of $Li_4Ti_5O_{12}$ anode batteries up to now.

* Corresponding authors at: Key Laboratory of Thermal Management Engineering and Materials, Graduate School at Shenzhen, Tsinghua University, Shenzhen 518055, China. Tel.: +86 755 26036118; fax: +86 755 26036118.
E-mail addresses: qhyangcn@tju.edu.cn (Q.-H. Yang), fykang@mail.tsinghua.edu.cn (F. Kang).

0378-7753/$ – see front matter © 2011 Elsevier B.V. All rights reserved.
doi:10.1016/j.jpowsour.2011.11.037

Some researchers reported that $Li_4Ti_5O_{12}$ can be discharged to a low voltage of 0 V, which can improve the specific capacity and rate discharge performance and does not influence the cycling performance of the material [11,23–26]. The energy density of $Li_4Ti_5O_{12}$ anode batteries therefore increases when the $Li_4Ti_5O_{12}$ anode is discharged to 0 V. It is well-known that most of the organic electrolytes have high reduction reactivity on the anode within the voltage range of 1–0.5 V, which can be reduced on the anode to form the SEI film. Meanwhile, a large number of gases such as CH_4, C_2H_4, C_2H_6, CO and CO_2, which depend on the components of electrolyte, are generated in this process [27,28]. Thus, the removal of gases is a necessary step after the formation of commercial batteries. The SEI film can also be formed when the $Li_4Ti_5O_{12}$ electrode is discharged to low potentials (below 1 V). Shu reported that the organic lithium alkylcarbonates were the primary component of SEI film formed during the reduction process [29], which was similar to that of SEI film of carbon anode [28,30]. For the $Li_4Ti_5O_{12}$ anode batteries, the potential of $Li_4Ti_5O_{12}$ anode may decline to below 1 V due to the polarization when the batteries are fully charged, especially with a high charge current. The electrolyte can also be reduced on the $Li_4Ti_5O_{12}$ anode during formation and cycling. Therefore, it is necessary and important to study the reduction reactivity of electrolyte on the $Li_4Ti_5O_{12}$ electrode below 1 V to understand and prevent the gas generation of $Li_4Ti_5O_{12}$ anode batteries.

In our previous work [31], we prepared the $Li_4Ti_5O_{12}$/C materials using amorphous TiO_2 by solid state method and then extensively investigated the effects of carbon addition in the precursors of amorphous TiO_2 and Li_2CO_3 on the rate and cycling performance of $Li_4Ti_5O_{12}$/C within the voltage range of 2.5–1 V. In this paper, we further investigated the reduction reactivity of electrolyte on uncoated and carbon-coated $Li_4Ti_5O_{12}$ electrodes and analyzed the effects of carbon, SEI film and impurity phase on the reduction reactivity of electrolyte for the first time. We found that the electrolyte shows high reduction reactivity on the pure $Li_4Ti_5O_{12}$ electrode, which is always reduced at around 0.7 V during $Li_4Ti_5O_{12}$ cycling between 2.5 V and 0 V. Whereas, the electrolyte is only reduced at the first cycle on the carbon-coated $Li_4Ti_5O_{12}$ electrode. Thus, carbon coating on the surface of $Li_4Ti_5O_{12}$ particles is an effective way to suppress the reduction decomposition of electrolyte on the $Li_4Ti_5O_{12}$ electrode. We also found the impurity phase such as rutile and anatase TiO_2 does not significantly influence the reduction reactivity of electrolyte. This work is of great importance to understand and solve the gas generation problem of $Li_4Ti_5O_{12}$ anode batteries.

2. Experimental

2.1. Preparation of $Li_4Ti_5O_{12}$ and $Li_4Ti_5O_{12}$/C materials

The saturated solution of cetyltrimethylammonium bromide (CTAB) (Tianjin Guangfu, China) was prepared using the deionized water under continuous stirring for 2 h. Then, the butyl titanate ($Ti(OC_4H_9)_4$) (Kermel, China) was added into the CTAB solution under ultrasound vibration, and then the stoichiometric ammonia was added under ultrasound for 15 min and continuous stirring for 4 h. The solution of nano-amorphous TiO_2 was filtrated and dried, and then the nano-amorphous TiO_2 was obtained. The filtration products of amorphous TiO_2 could not be washed completely with the deionized water, and some CTAB still existed in the amorphous TiO_2 nanoparticles.

$Li_4Ti_5O_{12}$ was synthesized using above prepared amorphous TiO_2 and Li_2CO_3 by solid-state method. The precursors of amorphous TiO_2 and Li_2CO_3 (Tianjin Guangfu, China) were mixed and the molar ratio of Li:Ti was 4.2:5. The precursors were ground for 6 h by wet ball-milling in an acetone solution. The resulting stable gel was dried at 80 °C to form a mixed dry precursor. The dried powder precursor was then calcinated at 800 °C for 12 h in air atmosphere using Tubular furnace (Central furnace, China). The $Li_4Ti_5O_{12}$/C composite materials were also prepared by a similar solid-state method as mentioned above using a precursor mixture of amorphous TiO_2, Li_2CO_3 and glucose in argon atmosphere. The thermogravimetric (TG) measurements for precursors of the amorphous TiO_2, Li_2CO_3 and glucose at air and argon atmospheres were conducted with a heating rate of 10 °C min^{-1} from room temperature to 800 °C by using a Rigaku Thermo Plus TG8120 system (Rigaku Corp., Japan).

2.2. Sample structure and morphology characterization

X-ray diffraction (XRD) patterns of the $Li_4Ti_5O_{12}$ and $Li_4Ti_5O_{12}$/C materials were obtained by a Rigaku D/max 2500/PC diffractometer (Rigaku Corp., Japan) using Cu Kα radiation in an angular range of 10–90° (2θ) with a 0.02° (2θ) step. Raman spectroscopy was performed with a Raman Spectrometer (Renishaw Invia Reflex, Britain) with a 514 nm Ar-ion laser. Microstructure and morphology of the prepared powders were observed with a field emission scanning electron microscopy (FE-SEM, HITACH S4800, HITACH Co., Japan) and transmission electron microscopy (TEM, JOEL JSM-2100F, Japan).

2.3. Cell assembly and testing

2032-type coin cells were prepared to study the reduction reactivity of electrolyte on the $Li_4Ti_5O_{12}$ and $Li_4Ti_5O_{12}$/C materials. The cells used $Li_4Ti_5O_{12}$ or $Li_4Ti_5O_{12}$/C composite as cathode material, lithium foil as anode, and polypropylene (Celgard 2500, Celgard Inc., USA) as separator. The cathode consisted of 80 wt.% $Li_4Ti_5O_{12}$/C composite, 10 wt.% Super-P and 10 wt.% poly(vinylidene fluoride) (PVDF). The active material loading of electrodes was about 7.5 mg cm^{-2}. 1 M $LiPF_6$ in a 1:1 mixture of ethylene carbonate and diethyl carbonate (1 M $LiPF_6$/EC + DEC) (Dongguan Shanshan Tech, China) was used as the electrolyte. The cells were assembled in a glove box (Mbraum, oxygen and moisture level less than 0.1 ppm) filled with high purity argon gas.

The electrochemical working station of VMP3 (Bio Logic Science Instruments, France) was used to measure the cyclic voltammograms (CV) and electrochemical impedance spectra (EIS) of cells. The CV test was used to characterize the reduction reactivity of electrolyte on the $Li_4Ti_5O_{12}$ and $Li_4Ti_5O_{12}$/C electrodes. The EIS test was used to testify the SEI film formation. EIS of the coin cells were measured at half state of charge using $Li_4Ti_5O_{12}$ or $Li_4Ti_5O_{12}$/C electrodes as the working electrode and lithium electrode as both the reference and counter electrodes. The impedance was measured by applying a 5 mV of ac oscillation with the frequency ranging from 100 kHz to 0.01 Hz. The CV of coin cells were performed with $Li_4Ti_5O_{12}$ or $Li_4Ti_5O_{12}$/C electrodes as the working electrode, lithium coil as both the reference and counter electrodes. A scanning rate of 0.1 mV s^{-1} was applied.

The coin cells before and after CV were transferred to a glove box and then dissembled. The $Li_4Ti_5O_{12}$ electrode was rinsed using dimethyl carbonate (DMC) to remove the electrolyte from the electrode surface. Then, $Li_4Ti_5O_{12}$ electrode was dried in the glove box antechamber to remove the residual DMC. The surface morphology of electrode was examined with a field emission scanning electron microscopy and the surface compositions of electrode were analyzed using Fourier transform infrared spectroscopy (FT-IR) spectrometer (Bruker VERTEX 70). The charge and discharge tests of coin cells were performed using a Land 2001A cell test system (Wuhan Land, China) at room temperature. The formation current density of $Li_4Ti_5O_{12}$ and $Li_4Ti_5O_{12}$/C electrodes is 17.5 mA g^{-1} (0.1 C).

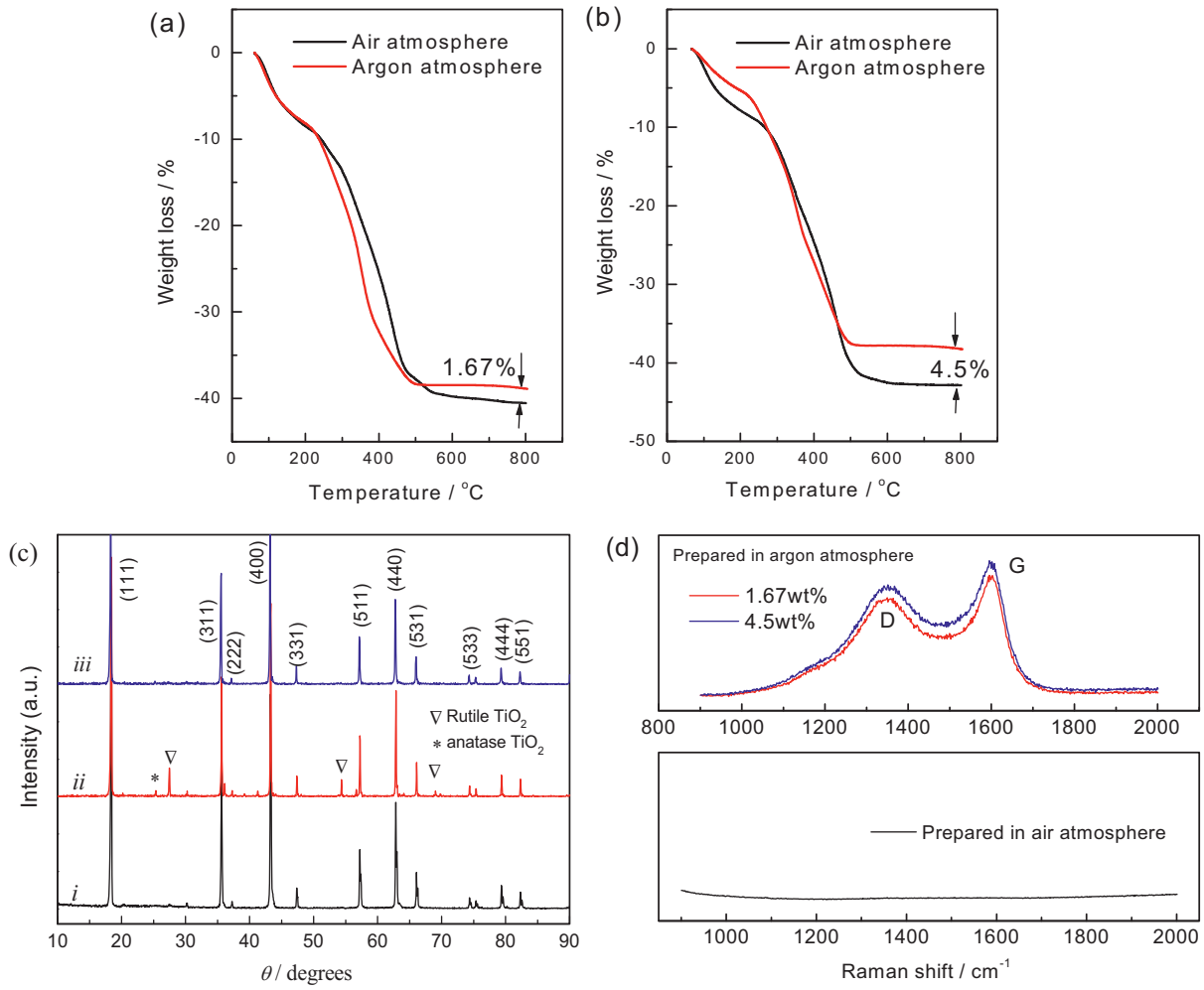

Fig. 1. TG curves of the precursors of amorphous TiO_2 and Li_2CO_3 (a) and amorphous TiO_2, Li_2CO_3 and glucose (b) in air and argon atmospheres; XRD patterns of $Li_4Ti_5O_{12}$ (*i*) and $Li_4Ti_5O_{12}$/C composite containing 1.67 wt.% carbon (*ii*) and 4.50 wt.% carbon (*iii*) (c); Raman spectra of $Li_4Ti_5O_{12}$ prepared in air atmosphere and $Li_4Ti_5O_{12}$/C composite containing 1.67 wt.% carbon and 4.50 wt.% carbon prepared in argon atmosphere (d).

3. Results and discussion

Fig. 1a shows the TG curves of precursors of amorphous TiO_2 containing CTAB and Li_2CO_3 in air and argon atmospheres. It can be seen that the amount of residual carbon in the $Li_4Ti_5O_{12}$ material in argon atmosphere is about 1.67 wt.% due to the CTAB decomposition at argon atmosphere. Fig. 1b presents the TG curves of precursors of amorphous TiO_2 containing CTAB, Li_2CO_3 and glucose in air and argon atmospheres. It can be observed that the carbon content in the $Li_4Ti_5O_{12}$/C composite material is 4.5 wt.%.

The XRD patterns of $Li_4Ti_5O_{12}$ and $Li_4Ti_5O_{12}$/C materials are shown in Fig. 1c. It can be seen from Fig. 1c(*i*) that the XRD pattern of $Li_4Ti_5O_{12}$ is in good agreement with JCPDS file (card No. 26-1198), confirming the formation of pure $Li_4Ti_5O_{12}$ using the precursors of amorphous TiO_2 and Li_2CO_3 at air atmosphere. The diffraction peaks can be indexed with the spinel structure of $Li_4Ti_5O_{12}$ with the space group *Fd*3*m*. As shown in Fig. 1c(*ii*) and (*iii*), the crystal structure of the samples synthesized at argon atmosphere changes significantly with the increase in the carbon content. The XRD patterns of $Li_4Ti_5O_{12}$ containing 1.67 wt.% carbon show obvious impurity phase peaks of rutile and anatase TiO_2, whereas the XRD patterns of $Li_4Ti_5O_{12}$ containing 4.5 wt.% carbon do not contain the impurity phase peaks. This may be due to that the use of glucose in the synthesis of $Li_4Ti_5O_{12}$/C would serve to enrich the oxygen content in the reactor and also to enhance the intermixing between the precursors of TiO_2 and Li_2CO_3. This suggests that the glucose as carbon sources added in the precursors of amorphous TiO_2 and Li_2CO_3 plays an important role in controlling the impurity phases of anatase and rutile TiO_2. It also can be seen from the XRD patterns of the $Li_4Ti_5O_{12}$/C composite that no diffraction response of carbon is observed.

In order to determine the state of carbon, the Raman spectrum of samples is examined. Fig. 1d shows the Raman spectra of $Li_4Ti_5O_{12}$ and $Li_4Ti_5O_{12}$/C synthesized at air and argon atmospheres. Two main bands are observed at around 1365 and 1594 cm^{-1} in the Raman spectra of $Li_4Ti_5O_{12}$/C, which are designated as the D band and G band, respectively. The G-peak corresponds to graphite in-plane vibrations with E_{2g} symmetry, and the D-peak is generally associated with a double-resonance effect [22,32]. The value I_D/I_G (the peak intensity ratio) can be used to evaluate the degree of disorder for the pyrolytic carbon. The low values for the I_D/I_G parameter indicate a high degree of graphitization. The values of the I_D/I_G for $Li_4Ti_5O_{12}$/C containing 1.67 and 4.5 wt.% carbon are respective 2.48 and 2.47, which suggest that the carbon is mainly in amorphous state.

As shown in Fig. 2a, the specific capacity of $Li_4Ti_5O_{12}$ electrode discharged to 1 and 0 V is above 160 and 240 mAh g^{-1}, respectively, and the material shows good reversibility. This indicates that the $Li_4Ti_5O_{12}$ material has good electrochemical performance.

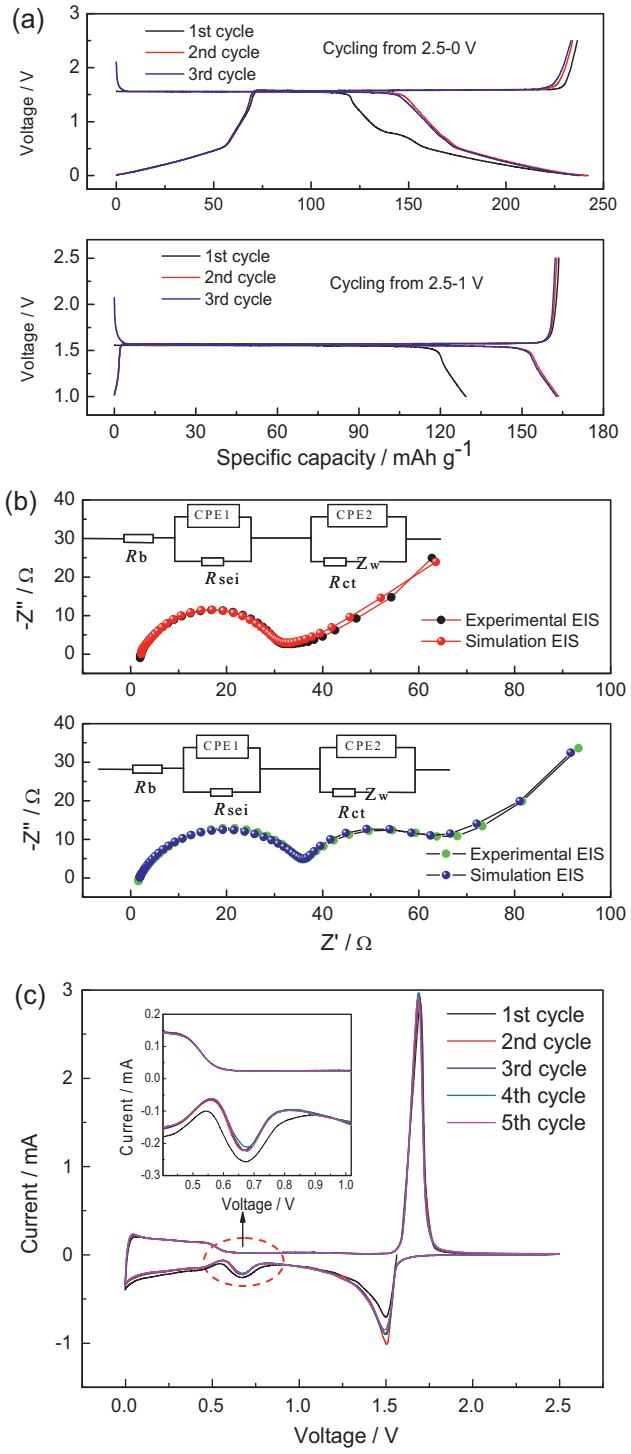

Fig. 2. Charge and discharge curves of $Li_4Ti_5O_{12}$ electrode (a), EIS and CV curves of $Li_4Ti_5O_{12}$ electrode (b, c).

The EIS results of $Li_4Ti_5O_{12}$/Li half cells after the formation in the voltage ranges of 2.5–0 V and 2.5–1 V are plotted in Fig. 2b. It can be seen that the EIS of $Li_4Ti_5O_{12}$ electrode after the formation from 2.5 to 1 V seems to be composed of only one depressed semicircle at high to middle frequency and a slope line at low frequency, whereas the EIS of $Li_4Ti_5O_{12}$ electrode after the formation between 2.5 and 0 V is composed of two partially overlapped and depressed semicircles at high to middle frequency and a slope line at low frequency. All cells were cycled 3 times before the EIS measurement to ensure a complete formation of $Li_4Ti_5O_{12}$ electrode. As shown in Fig. 2b,

Table 1
Values of the R_b, R_{sei} and R_{ct} obtained by simulating the data of Fig. 2b.

Resistance	R_b (Ω)	R_{sei} (Ω)	R_{ct} (Ω)
Formation 2.5–1 V	2.24	1.65	22.53
Formation 2.5–0 V	1.87	35.06	22.00

the EIS was simulated by Z-view software using same equivalent circuit. It can be observed that the experimental and simulated EIS are almost coincident, which indicates that the EIS of the $Li_4Ti_5O_{12}$ electrode formation in the voltage ranges of 2.5–0 V and 2.5–1 V all fit the equivalent circuit. According to the equivalent circuit, the EIS of the depressed semicircle at high frequency is attributed to the resistance (R_{sei}) and CPE1 of the solid electrolyte interface, and the depressed semicircle at medium frequency is attributed to the charge-transfer resistance (R_{ct}) and CPE2. Instead of capacitance (C_{sei}) of the solid electrolyte and double-layer capacitance (C_{dl}), the constant phase elements of CPE1 and CPE2 are used to take into account the roughness of the particle surface [33–36]. The slope line at low frequency corresponds to the Warburg impedance (Z_w), which is related to the lithium ion diffusion within the particles. It can be obtained from the simulation results of Table 1 that the R_{sei} of the $Li_4Ti_5O_{12}$ electrode formation in the voltage range of 2.5–0 V is 35.06 Ω, which is much larger than that in the voltage range of 2.5–1 V of 1.65 Ω. This proves that a relatively thick SEI film is formed on the $Li_4Ti_5O_{12}$ electrode from 2.5 to 0 V, whereas only a very thin SEI film can be formed on the $Li_4Ti_5O_{12}$ electrode formation between 2.5 and 1 V. Moreover, the R_{ct} of $Li_4Ti_5O_{12}$ electrode formation from 2.5 to 1 V (22.53 Ω) is much larger than the R_{sei} (1.65 Ω), thus, only one depressed semicircle at high to middle frequency seems to be observed in the EIS of $Li_4Ti_5O_{12}$ electrode after the formation from 2.5 to 1 V. It also can be seen that the R_{sei} of the $Li_4Ti_5O_{12}$ electrode formation in the voltage range of 2.5–0 V is even larger than the R_{ct} (22.00 Ω), which indicates that the SEI film formed on the $Li_4Ti_5O_{12}$ electrode has a relatively larger resistance as compared with that of the graphite anode [37]. Whereas, the R_{ct} for the $Li_4Ti_5O_{12}$ electrode formation between 2.5 and 1 V is 22.53 Ω, which is similar with that of 22.00 Ω for the formation in the voltage range of 2.5–0 V.

The CV profile of $Li_4Ti_5O_{12}$ between 2.0 and 0 V is shown in Fig. 2c. The cathodic and anodic peaks at respective 1.75 and 1.45 V are attributed to the redox of Ti^{4+}/Ti^{3+}, and the reduction and oxidation peaks below 0.6 V are caused by a multi step restore of Ti^{4+} [23,26]. It is interesting to note that an obvious irreversible peak appears at around 0.7 V during reduction process. This is due to the electroreductive formation of SEI film on the $Li_4Ti_5O_{12}$. Gases are also produced in the process of electrolyte reduction decomposition to form the SEI film. In this work, we used 1 M $LiPF_6$/EC + DEC as the electrolyte. Thus, the following reduction decomposition reactions may occur during the SEI film formation [27,28,38]:

$$EC: (CH_2O)_2CO + 2Li^+ + 2e^- \rightarrow (CH_2OLi) + CO(g) \quad (1)$$

$$DEC: C_2H_5OCO_2C_2H_5 + 2Li^+ + 2e^- \rightarrow CH_3CH_2OLi + CO(g) \quad (2)$$

$$EC: (CH_2O)_2CO + 2Li^+ + 2e^- \rightarrow Li_2CO_3 + C_2H_4(g) \quad (3)$$

$$DEC: C_2H_5OCO_2C_2H_5 + 2Li^+ + 2e^- \rightarrow Li_2CO_3 + C_4H_{10}(g) \quad (4)$$

$$EC: 2(CH_2O)_2CO + 2Li^+ + 2e^- \rightarrow (CH_2OCO_2Li)_2 + C_2H_4(g) \quad (5)$$

The surface compositions of electrode were anlysized to confirm the SEI Film formation using the FT-IR spectrometer. Fig. 3 presents the FT-IR spectra of PVDF, $Li_4Ti_5O_{12}$ and $Li_4Ti_5O_{12}$/C powders and electrodes before and after CV. It can be seen that the peaks of PVDF below 1400 cm^{-1} is complex. Thus, it is difficult to confirm the electrode surface compositions from peaks of below 1400 cm^{-1}. Whereas, from the peaks of above 1400 cm^{-1}, the compositions of $(CH_2OCO_2\ Li)_2$ (1624 cm^{-1}) and Li_2CO_3 (1500 cm^{-1})

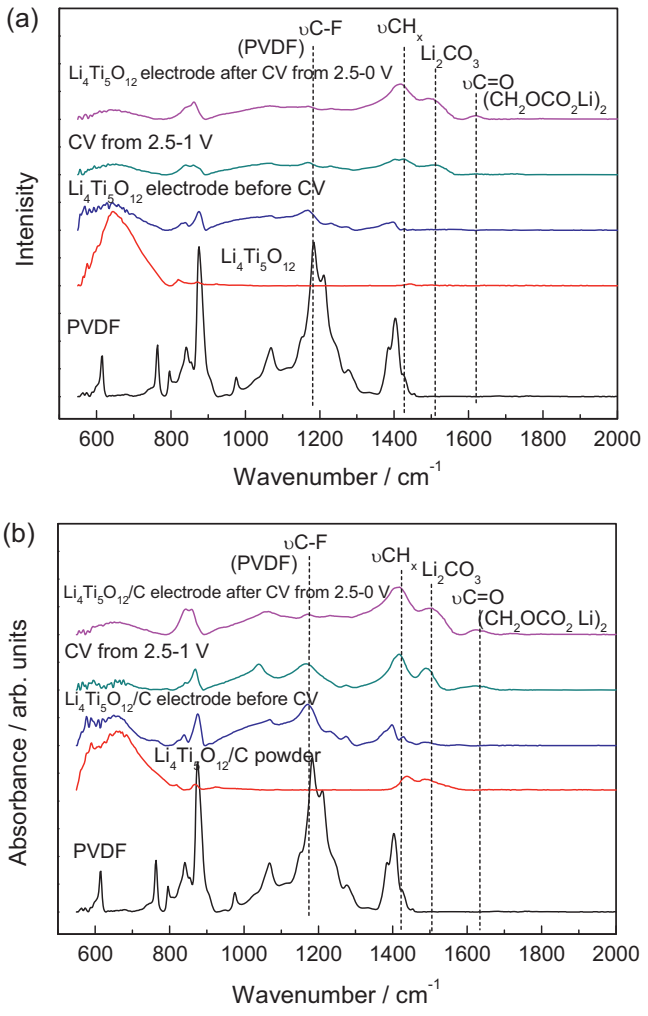

Fig. 3. FT-IR spectra of PVDF, $Li_4Ti_5O_{12}$ (a) and $Li_4Ti_5O_{12}$/C with 4.5 wt.% carbon (b) powders and electrodes before and after CV.

can be detected [39–41]. This suggests that above proposed reactions of 3–5 occur. All $Li_4Ti_5O_{12}$ and $Li_4Ti_5O_{12}$/C electrodes before and after formation contain the binder of PVDF and moreover, the typical peak of ROLi at around 1050 cm^{-1} is similar with that of C–F. Therefore, the ROLi cannot be identified from the FT-IR spectra. However, the reactions of 1–2 have been confirmed by many previous reports [27,28,38]. In addition, the peak intensity of $Li_4Ti_5O_{12}$/C electrode after formation is larger than that of $Li_4Ti_5O_{12}$ electrode, which indicates that the SEI film is more easily formed on the $Li_4Ti_5O_{12}$/C electrode. It also can be found that the SEI film compositions of electrode for the formation from 2.5 to 0 V are similar with that from 2.5 to 1 V.

For the carbon anode, the SEI film is mainly formed in the first cycle, and the irreversible peak on the CV curves almost disappears after the first cycle [37], whereas the irreversible peak at around 0.7 V on the CV curves of $Li_4Ti_5O_{12}$ electrode does not disappear from the second cycle. This indicates that the reduction decomposition reaction of electrolyte further occurs on the $Li_4Ti_5O_{12}$ electrode after the first cycle, which suggests that the electrolyte shows high reduction reactivity on the $Li_4Ti_5O_{12}$ material synthesized in air condition and the gases such as CO, C_2H_4 and C_4H_{10} are still generated during cycling. The SEI film formed on $Li_4Ti_5O_{12}$ particles cannot suppress the further reduction decomposition of electrolyte. This may be the main reason for the gas generation of $Li_4Ti_5O_{12}$ electrode during cycling. However, it is noted that the irreversible reduction reaction of electrolyte on the $Li_4Ti_5O_{12}$/C composite at around 0.7 V only occurs in the first cycle as shown in Fig. 4a and b. This indicates that the further irreversible reduction reactions of electrolyte after the first cycle are suppressed, even for the $Li_4Ti_5O_{12}$/C composite containing only 1.67 wt.% carbon. It can be seen from Fig. 4c that the EIS of the $Li_4Ti_5O_{12}$/C electrode formation between 2.5 and 0 V also contains two partially overlapped and depressed semicircles at high to middle frequency, whereas the EIS of the $Li_4Ti_5O_{12}$/C electrode after the formation from 2.5 to 1 V seems to be only composed of one depressed semicircle at high to middle frequency (see Fig. 4d).

Table 2
Values of the R_b, R_{sei} and R_{ct} obtained by simulating the data of Fig. 4c and d.

Carbon content	Resistance	R_b (Ω)	R_{sei} (Ω)	R_{ct} (Ω)
1.67 wt.%	Formation 2.5–1 V	1.91	5.20	23.51
	Formation 2.5–0 V	1.61	61.86	41.93
4.5 wt.%	Formation 2.5–1 V	1.74	3.32	16.48
	Formation 2.5–0 V	1.88	78.85	52.11

The EIS were also simulated by Z-view software as shown Fig. 2b. Table 2 shows the simulating results. It can be seen that the R_{sei} of the $Li_4Ti_5O_{12}$/C electrode formation in the voltage ranges of 2.5–0 V is much larger than that of formation from 2.5 to 1 V. This suggests that a relatively thick SEI film is also formed on the $Li_4Ti_5O_{12}$/C electrode during the formation between 2.5 and 0 V and the SEI film can prevent the further reduction decomposition of electrolyte, whereas only a thin SEI film can be formed on the $Li_4Ti_5O_{12}$/C electrode during the formation between 2.5 and 1 V. For the $Li_4Ti_5O_{12}$/C electrode formation in the voltage range of 2.5–0 V, the R_{sei} increases from 61.86 to 78.85 Ω and the R_{ct} increases from 41.93 to 52.11 Ω with the carbon content increasing from 1.67 to 4.5 wt.%, whereas the R_{ct} decreases from 23.51 to 16.48 Ω when the $Li_4Ti_5O_{12}$/C electrode is formed between 2.5 and 1 V. It is also found that the R_{ct} rises greatly after the formation in the voltage range of 2.5–0 V. Therefore, as shown in Fig. 4a and b, the reversibility of the $Li_4Ti_5O_{12}$/C composite between 2.5 and 0 V becomes worse with the increase in carbon content. The $Li_4Ti_5O_{12}$/C composite cycled between 2.5 and 0 V also shows worse reversibility as compared with that cycled in the voltage range of 2.5–1 V (see Fig. 4e and f). It can be concluded that a proper carbon content in the $Li_4Ti_5O_{12}$/C composite is needed, which can suppress the reduction decomposition of electrolyte and does not cause a great increase of R_{sei} and R_{ct}.

Fig. 4e shows that the specific capacity of the $Li_4Ti_5O_{12}$/C composite containing 1.67 wt.% carbon discharged to 1 and 0 V is 158 and 245 mAh g^{-1}, respectively, and Fig. 4f presents that the specific capacity of the $Li_4Ti_5O_{12}$/C composite containing 4.5 wt.% carbon discharged to 1 and 0 V is respective 168 and 245 mAh g^{-1}. This indicates that the $Li_4Ti_5O_{12}$/C composite with 1.67 wt.% carbon, which contains impurity phases such as rutile and anatase TiO_2, has a relatively lower specific capacity as compared with that of the uncoated material and the material with 4.5 wt.% carbon.

From the above analysis, we have found that the electrolyte shows much less reduction reactivity on the $Li_4Ti_5O_{12}$/C composite electrode than that on the $Li_4Ti_5O_{12}$ electrode after the first cycle. Fig. 2b and c have shown that the SEI film can be formed on the $Li_4Ti_5O_{12}$ electrode cycled from 2.5 to 0 V, whereas the reduction reaction of electrolyte on the $Li_4Ti_5O_{12}$ electrode still occurs after the first cycle. However, for the $Li_4Ti_5O_{12}$/C composite electrode, the reduction reaction of electrolyte only occurs at the first cycle (see Fig. 4a and b), which indicates that the SEI film on the $Li_4Ti_5O_{12}$/C composite electrode is almost formed completely during the first cycle. This is quite different to the SEI film formation on the pure $Li_4Ti_5O_{12}$ electrode.

The SEM and TEM images of $Li_4Ti_5O_{12}$ as shown in Fig. 5a and b indicate that the $Li_4Ti_5O_{12}$ powder has a uniform and nearly cubic

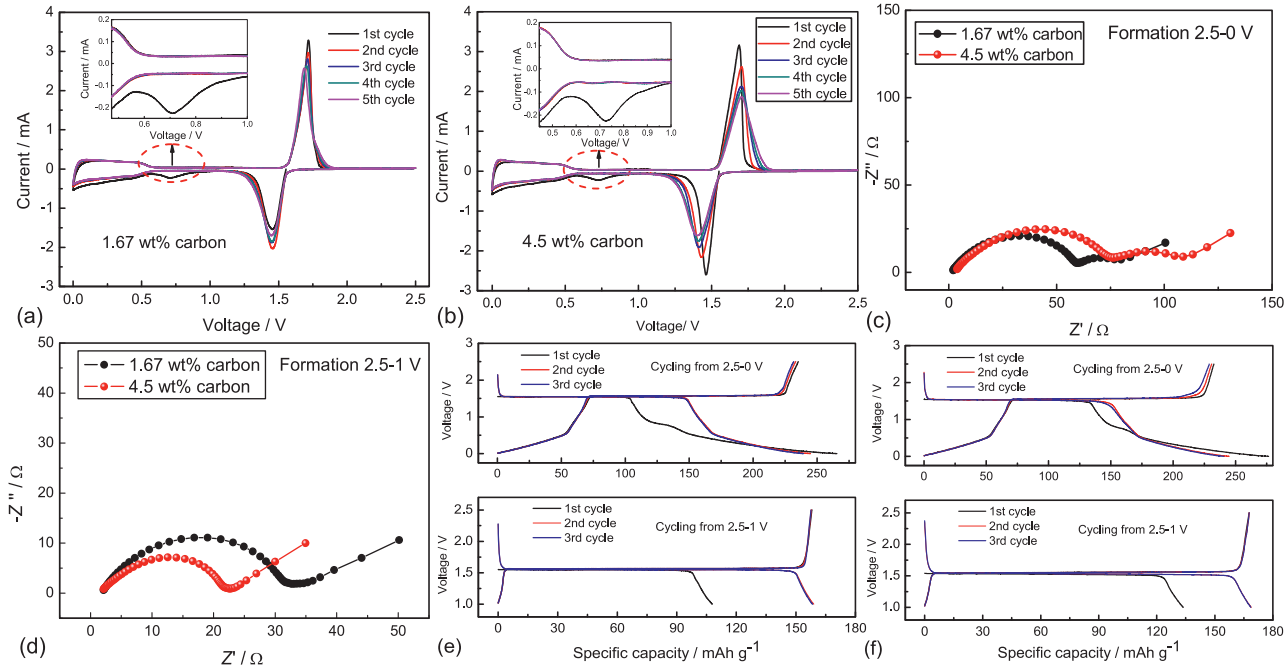

Fig. 4. CV (a, b), EIS (c, d) and charge and discharge (e, f) curves of $Li_4Ti_5O_{12}$/C composite containing 1.67 wt.% carbon and 4.5 wt.% carbon.

structural morphology with narrow size distribution of under 1 μm (see Fig. 5a) and well-crystallized structure (see Fig. 5b). Fig. 1c(*i*) also shows that the obtained powder samples are pure $Li_4Ti_5O_{12}$, and hardly contain impurity phases such as rutile and anatase TiO_2. The SEM images of the $Li_4Ti_5O_{12}$/C composites containing 1.67 and 4.5 wt.% carbon as shown in Fig. 5c and e indicate that the grain size of the as-prepared $Li_4Ti_5O_{12}$/C composite is less than 400 nm. Figs. 1d and 5c also show that the $Li_4Ti_5O_{12}$/C sample with 1.67 wt.% carbon contains free amorphous carbon. It can be seen from the XRD patterns in Fig. 1c(*ii*) that the sample also contains the rutile and anatase TiO_2. From the high resolution TEM image (Fig. 5d), it can be identified that the $Li_4Ti_5O_{12}$ particles are coated with a thin carbon layer with thickness of about 0.5 nm. For the $Li_4Ti_5O_{12}$/C sample containing 4.5 wt.% carbon, the $Li_4Ti_5O_{12}$ particles are covered by relatively thick surface layers (as shown in Fig. 5e). It can be seen from the high resolution TEM image (Fig. 5f) that several carbon layers with thickness of 2–5 nm and interlayer spacing of around 0.5 nm are uniformly coated on the well-crystallized $Li_4Ti_5O_{12}$ particles.

The surface morphology of $Li_4Ti_5O_{12}$/C with 4.5 wt.% carbon and $Li_4Ti_5O_{12}$ without carbon before and after CV was examined by SEM (see Fig. 6). It can be seen from Fig. 6a and b that a SEI film cannot be obviously observed on the surface of $Li_4Ti_5O_{12}$/C and $Li_4Ti_5O_{12}$ electrodes after CV from 2.5 to 1 V, which indicates that only a very thin SEI film is formed on the electrode surface. For the $Li_4Ti_5O_{12}$/C and $Li_4Ti_5O_{12}$ electrodes formation from 2.5 to

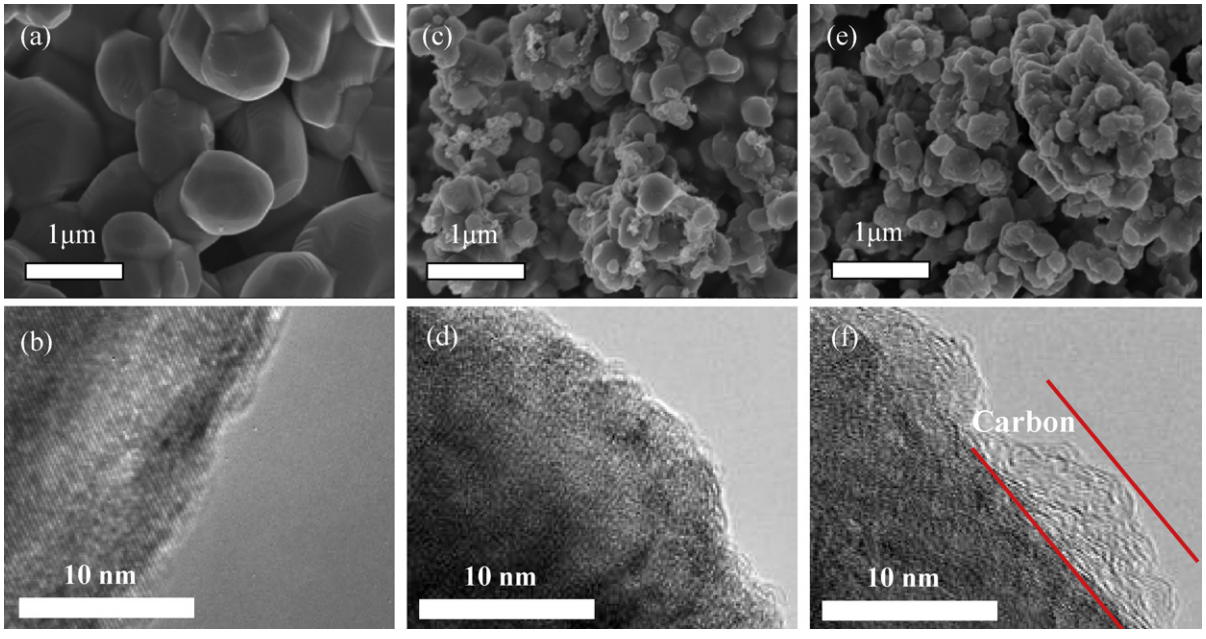

Fig. 5. SEM and TEM images of $Li_4Ti_5O_{12}$ (a, b) and $Li_4Ti_5O_{12}$/C composite containing 1.67 wt.% carbon (c, d) and 4.5 wt.% carbon (e, f).

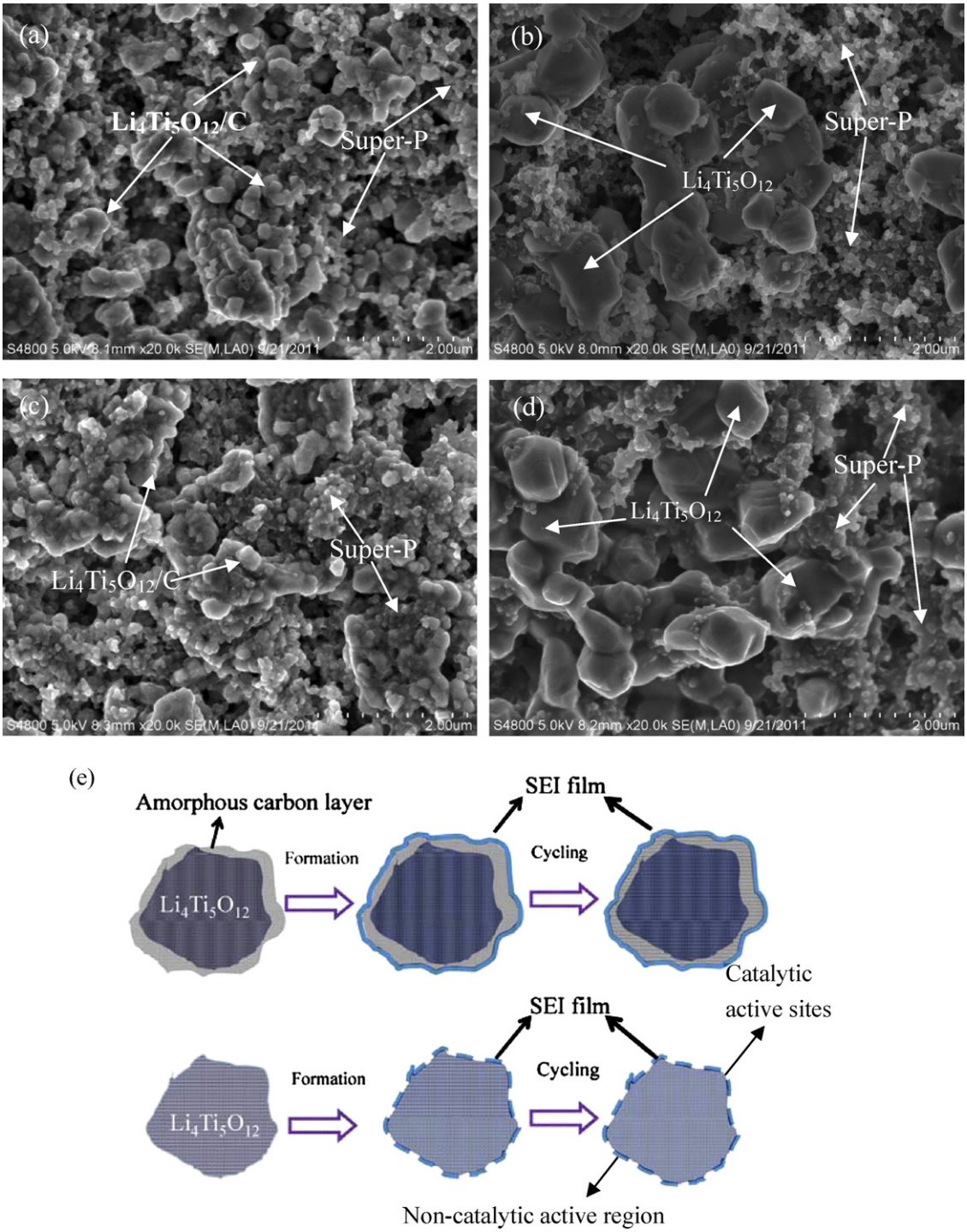

Fig. 6. SEM images of $Li_4Ti_5O_{12}$/C with 4.5 wt.% carbon and $Li_4Ti_5O_{12}$ without carbon electrodes after CV within the voltage range of 2.5–1 V (a, b) and 2.5–0 V(c, d), the SEI formation mechanism on $Li_4Ti_5O_{12}$ and $Li_4Ti_5O_{12}$/C composite electrodes during formation and cycling between 2.5 and 0 V (e).

0 V, the electrode surface shows different morphology (see Fig. 6c and d). It can be found that the $Li_4Ti_5O_{12}$/C electrode containing the $Li_4Ti_5O_{12}$/C and Super-P particles are all covered by a SEI film. However, For the $Li_4Ti_5O_{12}$ electrode, the Super-P particles are also covered by a SEI film, while the $Li_4Ti_5O_{12}$ particles seem not to be covered completely by a SEI film. All $Li_4Ti_5O_{12}$ particles are connected together at contact points and this behavior does not occur among $Li_4Ti_5O_{12}$ particles in the electrode after CV between 2.5 and 1 V. This may be because the SEI film is more easily formed at the contact points among $Li_4Ti_5O_{12}$ particles and they are connected together by the reduction decomposition products of electrolyte. In addition, it can be found that the spinel morphology of the $Li_4Ti_5O_{12}$ particles after CV from 2.5 to 0 V is less obvious than that after CV from 2.5 to 1 V, which suggests that some SEI film is also formed on the surface of $Li_4Ti_5O_{12}$ particles after CV from 2.5 to 0 V. Whereas, the SEI film formed on the $Li_4Ti_5O_{12}$ particles may be thinner and has richer pores than that on the $Li_4Ti_5O_{12}$/C particles, which results in the much less R_{sei} of $Li_4Ti_5O_{12}$ electrode than that of $Li_4Ti_5O_{12}$/C as shown in Figs. 2b and 4c.

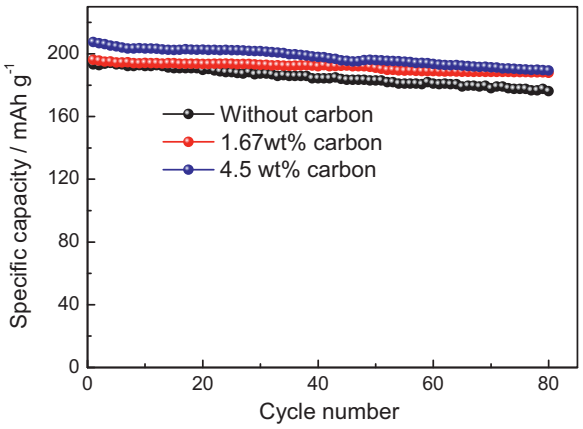

Fig. 7. Cycling performance of $Li_4Ti_5O_{12}$ and $Li_4Ti_5O_{12}$/C electrodes discharged to 0 V using charge rate of 0.5 C and discharge rate of 10 C.

As the gases are evolved during the formation of SEI film, large pores must be expected on the film, which are open ways for a new reduction of electrolyte in contact with C or $Li_4Ti_5O_{12}$ surfaces. From Fig. 2c, it can be obtained that the current of irreversible reduction reaction of electrolyte on the $Li_4Ti_5O_{12}$ electrode in the first CV at around 0.7 V is larger than that of 2–5 CVs, while the current at around 0.7 V from 2nd to 5th CV is almost equal and does not decrease. This may be due to that the SEI film can be formed on the Super-P particles at the first CV, while which is only formed on the part surface of $Li_4Ti_5O_{12}$ particles and the SEI film has some pores (see Fig. 6e). The pores perhaps are the catalytic active sites of $Li_4Ti_5O_{12}$ particles. The continuous reduction decomposition of electrolyte may be attributed to the catalytic activity of the $Li_4Ti_5O_{12}$ material. The SEI film formed on the $Li_4Ti_5O_{12}$ electrode does not totally cover the catalytic active sites of $Li_4Ti_5O_{12}$ particles after formation (as shown in Fig. 6e). The reduction decomposition products of organic lithium alkylcarbonates may be deposited on the non-catalytic active region to form a discontinuous SEI film with rich pores (as shown in Fig. 6e). Thus, the reduction decomposition reactions of electrolyte further occur at around 0.7 V on the catalytic active sites of $Li_4Ti_5O_{12}$ particles uncovered by a SEI film during cycling from 2.5 to 0 V. The further reduction decomposition products may be dissolved in the electrolyte and the pores of the SEI film may not close, which leads to poor cycling performance of cells.

However, for the $Li_4Ti_5O_{12}$/C electrode, the $Li_4Ti_5O_{12}$ particles are coated by amorphous carbon and the catalytic active sites of $Li_4Ti_5O_{12}$ particles are covered by the carbon layers. The composite electrode shows the characteristics of carbon electrode to some extent. A fast film formation accounts onto C and the pores are closed after the first discharge. Thus, the electrolyte does not contact with the $Li_4Ti_5O_{12}$/C electrode and the reduction reaction of electrolyte on the electrode does not occur. As shown in Fig. 6e, a successive SEI film can be formed on the carbon layer during the formation, which prevents the further reduction decomposition at around 0.7 V during cycling between 2.5 and 0 V. Therefore, the coated carbon layer plays a key role in suppressing the reduction decomposition of electrolyte on the $Li_4Ti_5O_{12}$ electrode, and just a very thin carbon film coated on $Li_4Ti_5O_{12}$ can suppress the further reduction decomposition of electrolyte during cycling. It is also found that the rutile and anatase TiO_2 in the $Li_4Ti_5O_{12}$/C composite has no obvious effect on the reduction reaction of electrolyte.

Fig. 7 shows the cycling performance of $Li_4Ti_5O_{12}$ and $Li_4Ti_5O_{12}$/C electrodes discharged to 0 V using charge rate of 0.5 C and discharge rate of 10 C. The capacity retention of $Li_4Ti_5O_{12}$/C with 1.67 and 4.5 wt.% carbon after 80 cycles are 95.72% and 91.27%, respectively. It can be seen that the cycling performance of $Li_4Ti_5O_{12}$/C electrode with discharge rate of 10 C between 2.5 and 0 V deteriorates with the carbon content increase from 1.67 to 4.5 wt.%, which may be due to the larger R_{sei} and R_{ct} as shown in Table 2. It also can be seen that the capacity retention of $Li_4Ti_5O_{12}$ electrode after 80 cycles is only 91.20%, which is much lower than that of $Li_4Ti_5O_{12}$/C electrode with 1.67 wt.% carbon. Thus, the carbon coated $Li_4Ti_5O_{12}$ electrode with proper carbon content shows much higher cycling stability, which may be attributed to that the carbon can suppress the reduction decomposition of electrolyte and reduce the consumption of electrolyte compared to the un-coated $Li_4Ti_5O_{12}$ electrode.

4. Conclusions

The uncoated and amorphous carbon-coated $Li_4Ti_5O_{12}$ materials with good electrochemical performance were prepared and the reduction reactivities of electrolyte on those electrodes were investigated. It is found that a relatively thick SEI film is formed on the uncoated and carbon-coated $Li_4Ti_5O_{12}$ electrodes after formation from 2.5 to 0 V, whereas only a very thin SEI film can be formed on them after formation between 2.5 and 1 V. The SEI film compositions of electrodes for the formation from 2.5 to 0 V are similar with that from 2.5 to 1 V. The R_{ct} of carbon-coated $Li_4Ti_5O_{12}$ electrode after the formation in the voltage range of 2.5–0 V is much larger than that in the formation voltage range of 2.5–1 V. The electrolyte shows quite different reduction reactivities on the un-coated $Li_4Ti_5O_{12}$ and carbon-coated $Li_4Ti_5O_{12}$ composite electrodes. The reduction decomposition reaction of electrolyte occurs at around 0.7 V on the uncoated $Li_4Ti_5O_{12}$ electrode during cycling from 2.5 to 0 V, whereas the same reaction only occurs at the first cycle on the carbon-coated $Li_4Ti_5O_{12}$ composite electrode. Carbon coating layer on the surface of $Li_4Ti_5O_{12}$ particles can cover the catalytic active sites and a successive SEI film can be formed on the carbon coating layer of the $Li_4Ti_5O_{12}$ particles. The $Li_4Ti_5O_{12}$/C electrode containing the $Li_4Ti_5O_{12}$/C and Super-P particles are all covered by a SEI film, which separates the catalytic active sites from the surrounding electrolyte and prevent the electrolyte from further reduction decomposition. Whereas, the SEI film formed on the $Li_4Ti_5O_{12}$ particles may be thinner and has richer pores than that on the $Li_4Ti_5O_{12}$/C particles, which are open ways for a new reduction of electrolyte in contact with $Li_4Ti_5O_{12}$ surfaces. Thus, the carbon coated $Li_4Ti_5O_{12}$ electrode with proper carbon content shows much higher cycling stability between 2.5 and 0 V compared to the uncoated $Li_4Ti_5O_{12}$ electrode. This work is of great importance for understanding and suppressing the reduction decomposition of electrolyte on the $Li_4Ti_5O_{12}$ electrode, especially when they are discharged to a very low working voltage to improve the energy density.

Acknowledgements

This work was supported by China Postdoctoral Science Foundation (No. 20100470296), National Nature Science Foundation of China (No. 50632040 and 51072131) and Shenzhen Technical Plan Project (No. JP200806230010A, No. SG200810150054A and JC201005310705A), and Guangdong Province Innovation R&D Team Plan for Energy and Environmental Materials.

References

[1] E. Ferg, R.J. Gummow, A.d. Kock, M.M. Thackeray, J. Electrochem. Soc. 141 (1994) L147.
[2] T. Ohzuku, A. Ueda, N. Yamamoto, J. Electrochem. Soc. 142 (1995) 1431.
[3] L. Aldon, P. Kubiak, M. Womes, J.C. Jumas, J. Olivier-Fourcade, J.L. Tirado, J.I. Corredor, C.P. Vicente, Chem. Mater. 16 (2004) 5721.
[4] S.S. Zhang, K. Xu, T.R. Jow, Electrochim. Acta 51 (2006) 1636.

[5] H. Schranzhofer, J. Bugajski, H.J. Santner, C. Korepp, K.-C. M¨oller, J.O. Besenhard, M. Winter, W. Sitte, J. Power Sources 153 (2006) 391.
[6] S.S. Zhang, K. Xu, T.R. Jow, J. Power Sources 130 (2004) 281.
[7] T. Doi, Y. Iriyama, T. Abe, Z. Ogumi, Chem. Mater. 17 (2005) 1580.
[8] A. Guerfi, S. Sevigny, M. Lagace, P. Hovington, K. Kinoshita, K. Zaghib, J. Power Sources 119 (2003) 88.
[9] L. Cheng, H.-J. Liu, J.-J. Zhang, H.-M. Xiong, Y.-Y. Xia, J. Electrochem. Soc. 153 (2006) A1472.
[10] Y. Abe, E. Matsui, M. Senna, J. Phys. Chem. Solids 68 (2007) 681.
[11] T.F. Yi, J. Shu, Y.R. Zhu, X.D. Zhu, R.S. Zhu, A.N. Zhou, J. Power Sources 195 (2010) 285.
[12] D. Capsoni, M. Bini, V. Massarotti, P. Mustarelli, G. Chiodelli, C.B. Azzoni, M.C. Mozzati, L. Linati, S. Ferrari, Chem. Mater. 20 (2008) 4291.
[13] J. Wolfenstine, J.L. Allen, J. Power Sources 180 (2008) 582.
[14] S.H. Huang, Z.Y. Wen, X.J. Zhu, Z.H. Gu, Electrochem. Commun. 6 (2004) 1093.
[15] S. Huang, Z. Wen, B. Lin, J. Han, X. Xu, J. Alloys Compd. 457 (2008) 400.
[16] S. Ji, J. Zhang, W. Wang, Y. Huang, Z. Feng, Z. Zhang, Z. Tang, Mater. Chem. Phys. 123 (2010) 510.
[17] J. Wang, X.-M. Liu, H. Yang, X.-d. Shen, J. Alloys Compd. 509 (2011) 712.
[18] G.J. Wang, J. Gao, L.J. Fu, N.H. Zhao, Y.P. Wu, T. Takamura, J. Power Sources 174 (2007) 1109.
[19] J.J. Huang, Z.Y. Jiang, Electrochim. Acta 53 (2008) 7756.
[20] X. Li, M.Z. Qu, Y.J. Huai, Z.L. Yu, Electrochim. Acta 55 (2010) 2978.
[21] X. Li, M.Z. Qu, Z.L. Yu, Solid State Ionics 181 (2010) 635.
[22] T. Yuan, X. Yu, R. Cai, Y.K. Zhou, Z.P. Shao, J. Power Sources 195 (2010) 4997.
[23] H. Ge, N. Li, D.Y. Li, C.S. Dai, D.L. Wang, Electrochem. Commun. 10 (2008) 719.
[24] M. Venkateswarlu, C.H. Chen, J.S. Do, C.W. Lin, T.C. Chou, B.J. Hwang, J. Power Sources 146 (2005) 204.
[25] S.H. Huang, Z.Y. Wen, Z.H. Gu, X.J. Zhu, Electrochim. Acta 50 (2005) 4057.
[26] H. Ge, N. Li, D.Y. Li, C.S. Dai, D.L. Wang, J. Phys. Chem. C 113 (2009) 6324.
[27] J.-S. Shin, C.-H. Han, U.-H. Jung, S.-I. Lee, H.-J. Kim, K. Kim, J. Power Sources 109 (2002) 47.
[28] R. Dedryvère, H. Martinez, S. Leroy, D. Lemordant, F. Bonhomme, P. Biensan, D. Gonbeau, J. Power Sources 174 (2007) 462.
[29] J. Shu, Electrochem. Solid State 11 (2008) A238.
[30] E. Peleda, D. Golodnitsky, A. Ulusa, V. Yufita, Electrochim. Acta 50 (2004) 391.
[31] B. Li, F. Ning, Y.-B. He, H. Du, Q.-H. Yang, J. Ma, F. Kang, C.-T. Hsu, Int. J. Electrochem. Sci. 6 (2011) 3210.
[32] X.B. Hu, Z.J. Lin, K.R. Yang, Y.J. Huai, Z.H. Deng, Electrochim. Acta 56 (2011) 5046.
[33] F. Nobili, R. Tossici, F. Croce, B. Scrosati, R. Marassi, J. Power Sources 94 (2001) 238.
[34] F. Croce, F. Nobili, A. Deptula, W. Lada, R. Tossici, A. D'Epifanio, B. Scrosati, R. Marassi, Electrochem. Commun. 1 (1999) 605.
[35] M. Umeda, K. Dokko, Y. Fujita, M. Mohamedi, I. Uchida, J.R. Selman, Electrochim. Acta 47 (2001) 885.
[36] G.T.K. Fey, W.H. Yo, Y.C. Chang, J. Power Sources 105 (2002) 82.
[37] Y.-B. He, B. Li, Q.-H. Yang, H. Du, F. Kang, G.-W. Ling, Z.-Y. Tang, J. Solid State Electrochem. 15 (2011) 1977.
[38] H. Yoshida, T. Fukunaga, T. Hazama, M. Terasaki, M. Mizutani, M. Yamachi, J. Power Sources 68 (1997) 311.
[39] D. Aurbach, Y. Eineli, B. Markovsky, A. Zaban, S. Luski, Y. Carmeli, H. Yamin, J. Electrochem. Soc. 142 (1995) 2882.
[40] H. Ota, A. Kominato, W.-J. Chun, E. Yasukawa, S. Kasuya, J. Power Sources 119/121 (2003) 393.
[41] X. Wang, T. Hironaka, E. Hayashi, C. Yamada, H. Naito, G. Segami, Y. Sakiyama, Y. Takahashi, K. Kibe, J. Power Sources 168 (2007) 484.